Automation in Construction 121 (2021) 103415

Contents lists available at ScienceDirect

Automation in Construction

journal homepage: www.elsevier.com/locate/autcon

Robotic spray coating of self-sensing metakaolin geopolymer for concrete monitoring

Jack McAlorum [a,*], Marcus Perry [a], Christos Vlachakis [a], Lorena Biondi [a], Brenden Lavoie [b]

[a] Civil and Environmental Engineering Department, University of Strathclyde, Glasgow G1 1XJ, UK
[b] Department of Civil & Mineral Engineering, University of Toronto, Toronto, ON M5S 1A4, Canada

ARTICLE INFO

Keywords:
Robotic sensing
Multifunctional materials
Skin sensors
Alkali-activated materials
Metakaolin
Structural health monitoring

ABSTRACT

Sensors and new materials can support optimised concrete maintenance, and produce the data needed to justify new, low carbon structural designs. While these technologies are affordable, the process of manual installation in a construction context comes with acute and unfamiliar risks to productivity, personnel safety, and confidence in the quality of workmanship. The installation of smart materials using robotics could address some of these issues, but there are few proofs-of-concept at the time of writing. Here, we present a robotically controlled process for spray coating geopolymers — a class of self-sensing concrete repair materials. By tuning mix design, robotic toolpaths and spray dispenser parameters, we show reliable and automated spray coating of 250 mm^2 patches in a laboratory setting. The cured geopolymer has a compressive strength of 20 MPa, and a bond strength to the concrete substrate of 0.5 MPa. Electrical interrogation of patches, via a set of four electrodes, produces strain and temperature measurements of the underlying concrete substrate with resolutions of 1 $\mu\varepsilon$ and 0.2 °C, respectively. This demonstration multifunctional material deposition using robotics is a step towards remote, traceable, and low-risk technology deployment across civil engineering sectors. This could support more widespread adoption of novel concrete health monitoring and repair systems in future.

1. Introduction

The infrastructure of developed nations is increasingly being supported by deteriorating concrete structures [1–3]. Asset managers are struggling to optimise concrete maintenance, and despite a tendency to overdesign [4], concrete structures are failing more frequently, and costing more time and resources to recover [5,6].

These challenges can be partly addressed with informed, pro-active maintenance, and improved structural design [7], but this demands knowledge of real-time structural performance. Modern sensors and self-sensing materials can capture the required data, but their use in construction remains uncommon. This is because monitoring technologies:

- *Bear a high cost*: the sensors themselves are affordable, but their installation campaigns pose significant labour costs, risks to productivity, and risks to personnel.
- *Deliver uncertain returns*: sensor repeatability and robustness are largely dependant on the quality of workmanship during installation [8]. This is a problem: humans frequently make mistakes [9], and are poor at remembering those mistakes [10]. This has a pronounced impact on our confidence in using sensor data to make design and maintenance decisions, and could harm industry's image of otherwise promising technologies [11–13].

In future, robotics could tackle these issues by delivering remote, repeatable, traceable sensor installation at a fixed cost, even in harsh environments. To begin showing that this is feasible in a construction context, this paper outlines a proof-of-concept system for robotically spray-coating a self-sensing material, known as a geopolymer, onto concrete surfaces.

Geopolymers are a class of curable, alkali-activated materials that exhibit similar mechanical properties to ordinary Portland cement: there is an abundance of literature on their use as fire- and chloride- resistant concrete repair and coating systems [14–20]. Geopolymers also exhibit a reasonably high electrolytic conductivity (10^{-6}–10^{-3} S/cm) due to free metallic ions in their matrix [21–25], and this has allowed them to be used as sensors for concrete strain, temperature and moisture [26–31]. Conventional alternatives to geopolymer for this application are mostly based on epoxies or OPC grouts laced with carbon or metallic additives (powders, fibres, nanoparticles) [32–34]. The main disadvantages of

* Corresponding author.
E-mail address: jack.mcalorum@strath.ac.uk (J. McAlorum).

https://doi.org/10.1016/j.autcon.2020.103415
Received 7 April 2020; Received in revised form 1 September 2020; Accepted 14 September 2020
Available online 9 October 2020

these compared to geopolymers include [35–37]:

- they tend to have a larger carbon footprint
- solutions employing metallic additives are prohibited by British and European standards as they can lead to electrochemical cells with rebar and induce corrosion
- solutions employing nanoparticles are not currently scalable.

Nevertheless, the robotic spray-coating method developed in this work could also be utilized for automated deployment of these materials.

Additive manufacturing methods have been explored as a deployment method for geopolymers [38–41]. Robotics may provide a more flexible method of automation, with increased area and multi-orientation deposition. This is more suitable for in-situ applications to damaged structures, whereas additive manufacturing may be more suited to pre-cast manufacturing. It is worth noting, that both methods are viable solutions for automated deployment of geopolymers. Manually spray-coated geopolymers have previously been demonstrated as repairs and coatings [42–44], but to our knowledge, this is the first time that the automated spray-coating of geopolymer skin sensors has been demonstrated.

2. Materials and methods

2.1. Robotic spray coating process overview

The robot setup and procedure for geopolymer spray-coating are summarised in Fig. 1 and Fig. 2, respectively. The spray coater, mounted to the end of the six axis robot, is comprised of a progressive cavity extruder followed by an atomiser. The use of this dispensing method ensures precise and repeatable low-flow-rate spraying of high viscosity media. Geopolymer is fed into the screw cavity from a dispenser fit with air supply pressure of 1 bar. This ensures material flow into the screw cavity regardless of sprayer orientation.

Fig. 1a) shows the attachment of the spray dispenser to the robot and defines the x, y and z axes for toolpath control. An infrared sensor, attached to the robot head, is connected to the robot's input to control the proximity, $P = [3\text{ cm}, 40\text{ cm}]$, between the spray nozzle and concrete substrate. As outlined in Fig. 2, proximity is defined as a customisable user input, as is the data for the geometry of the square patch (its width, W and thickness H), the robot head speed S and the dot size of spray, D. As illustrated in Fig. 1b), the spray coating process is made up of fast, sweeping motions repeated over a number of spray coating layers, L.

Patches are robotically sprayed onto Ordinary Portland Cement (OPC) based concrete blocks, with a mix design of 10.5 kg sand, 13.35 kg of 10 mm aggregate, 7.5 kg OPC and 3.375 l of water. The cubes are then cured for 28 days at room temperature submerged in a water tank, as per British-European standards. Metal electrodes are inserted into the geopolymer patches after spraying to allow for electrical impedance measurements post curing. Patches are then thermally cured at 40 °C for 24 h to accelerate the curing process.

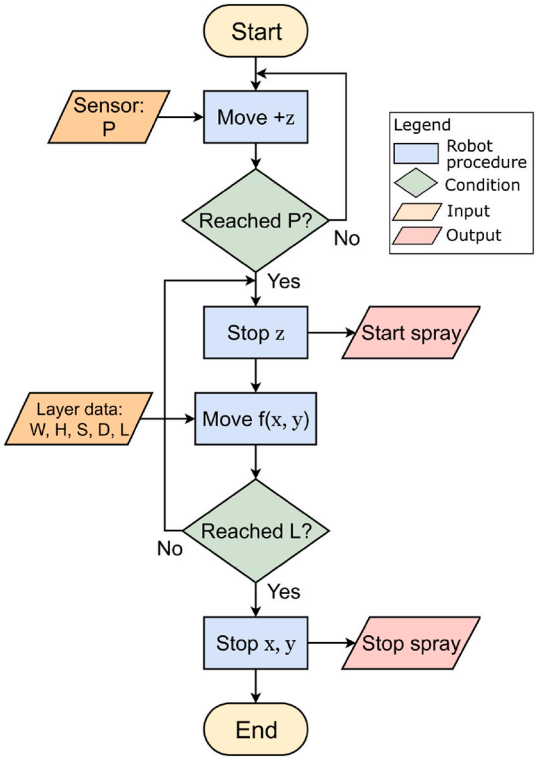

Fig. 2. Flow chart outlining the automated spray coating procedure.

2.2. Geopolymer mix design

Geopolymers are formulated by mixing an aluminosilicate precursor (such as metakaolin: china clay, calcined at temperatures of 550–850 °C), with an alkaline activator solution (comprised of e.g. a sodium hydroxide and sodium silicate solution mix) [45,46]. Upon mixing, a series of geopolymerisation reactions result in a workable

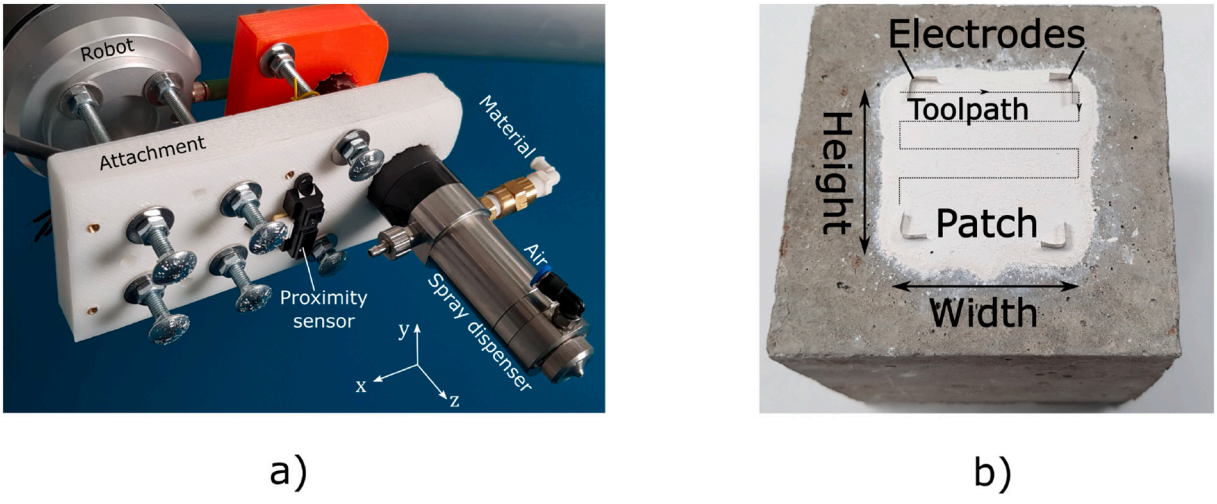

Fig. 1. a) Attachment of spray dispenser to robot head, with axis direction labelled. b) Concrete patch showing the toolpath used for spray coating.

binder that cures within 1–3 days at an elevated temperature of 40 °C [30,47], forming a strong bond with concrete substrates [48].

The mix design for the metakaolin geopolymer used throughout this work is outlined in Table 1. This mix defines many of its properties, from its behaviour during spraying, adhesion to the concrete substrate [49], ability to self-level, electrical conductivity [26] and mechanical strength [50]. At the time of writing, there are no accepted guidelines on geopolymer mix design. As such, trial and error was used to tune the mix design in this work, with the aim of targeting sprayability and coating integrity during curing.

Kaolin sourced from the Southwest of England, UK with 47% SiO_2, 38% Al_2O_3 and mean particle size 2 μm was calcined at 800 °C for 2 h to produce a metakaolin precursor [53]. The full process is provided in our previous work [54]. The properties of the metakaolin in this work, gained from an X-ray powder diffraction (XRD) test, are given in Table 2.

Metakaolin was chosen over other aluminosilicate precursor options (e.g. fly-ash, blast furnace slag) as its more consistent particle size provides more repeatable wet and cured properties during experimental optimisation [30].

The alkaline solution was a 2:1 ratio mix of sodium silicate to 10 M sodium hydroxide. The viscosity (and hence sprayability) of the material will mainly be governed by the solid/liquid (metakaolin/alkaline solution) ratio. Through a testing matrix, we identified that a solid/liquid ratio of 0.65 was most suitable for the particle spray dispenser described in Section 2.1.

2.3. Geopolymer additives

Previous work has shown that a moisture deficit within a curing geopolymer can cause cracking due to shrinkage [55], while excess water can lead to reduction of strength and efflorescence [14]. In most applications, water theft from the geopolymer into the concrete is the main issue. Common shrinkage reduction techniques include the addition of polypropylene or polyvinyl acetate (PVA) fibres [56–58], sand [59–61] or nano-TiO_2 particles [62]. In this work, several of these options were tried:

- at the reduced scale of our experiment, sand leads to clogging of the spray dispenser;
- replacing up to 0.5% of the solid content with colloidal silica nanoparticles was ineffective, as gelling of the particles caused misshapen patches after curing;
- PVA fibres [51,52] (0.1% by mass) were found to reduce shrinkage cracking without deleterious effects on spray coating.

To further counteract issues with water theft from the geopolymer, the concrete substrate was pre-wetted prior to spraying and samples were sealed to maintain an adequate moisture content during curing. At a larger scale, additives such as sand would be able to counteract drying shrinkage, negating the requirement to prewet the concrete or seal the samples.

2.4. Sensing principle

Geopolymer sensing works on the principle of measuring changes in the electrical impedance, $\overrightarrow{Z}$, of a geopolymer layer in response to measurands of interest. As illustrated in Fig. 3a, the impedance is found

Table 1
Geopolymer mix design.

Material	Wt%
Metakaolin	39.3
PVA fibres (3 mm Length) [51,52]	0.1
Sodium silicate solution	40.4
Sodium Hydroxide solution (10 M)	20.2

Table 2
Metakaolin properties.

Mineral (metakaolin powder)	Wt%
Amorphous content	87.0
Muscovite mica	9.5
Rutile	0.9
Quartz	2.6

by measuring the voltage response, $\overrightarrow{V}$ of the layer in response to an alternating (ac) current excitation, $\overrightarrow{I}$, of frequency, f, i.e. $\overrightarrow{I} = sin(2\pi ft)$:

$$\overrightarrow{Z} = \overrightarrow{V}\,\overrightarrow{\frac{1}{I}} = \frac{V}{I}e^{i(\phi_V - \phi_I)} = Ze^{i(\phi_V - \phi_I)}. \quad (1)$$

Here $\phi_V - \phi_I = 360f\Delta t$ is the phase (or time) offset between the measured voltage and applied current, $i = \sqrt{-1}$, and V, I and Z are the magnitudes of voltage, current and impedance, respectively. Fig. 3b shows a typical Nyquist plot for a spray coated patch, demonstrating the real and imaginary components of the impedance for various frequencies in the range f=[10 Hz, 1 MHz]. As geopolymers exhibit a capacitance, current lags voltage and the imaginary component of the impedance is negative.

A detailed explanation of how geopolymer impedance can be linked to measurands can be found in our previous work [31]. To summarise, the sensor's response to strain, ε and temperature, T, can typically be deduced from shifts in the magnitude of impedance, ΔZ, at a single ac frequency. The characterisation equation takes the form [63]:

$$\frac{\Delta Z}{Z_0} = \frac{Z - Z_0}{Z_0} = k_\varepsilon \varepsilon + exp\left(\frac{k_{T1}}{T} - k_{T2}T + k_{T0}\right), \quad (2)$$

where Z_0 is an arbitrary baseline impedance magnitude (taken at zero strain and ambient temperature) used to normalise for variations in geometry or baseline conductivity between sensor patches. Parametric constants k_ε, k_{T1}, k_{T2}, k_{T0} are found through characterisation.

In this work, the 4-electrode setup shown in Fig. 4 was used to assess the impedance of spray coated patches in response to temperature and an applied strain. This 4-electrode Van der Pauw configuration [64] is chosen as it reduces the influence of wire and contact resistances, and the interfacial stresses between electrodes and geopolymer exerted on the patches during curing. As patches are sensitive to strain, temperature and moisture, they will require compensation with reference sensors when deployed in the field.

2.5. Thermal and mechanical characterisation

Cured patches were placed in an environmental chamber and cycled between 10 °C and 30 °C in steps of 5 °C to characterise the sensor response to temperature. Samples were held at each temperature for 2 h to ensure thermal equilibrium of the concrete while the electrical impedance was measured.

Patches were also tested under compressive load, as shown in Fig. 5a). Uniaxial compressive forces of up to 8 kN were applied to the host concrete cube in steps of 2 kN.

Experiments were also carried out to determine the compressive strength of the geopolymer mix design itself, and its adhesion strength to the concrete substrate. Cubes of the same geopolymer paste mix (side length 30 mm) were cast and placed under compressive testing during a 28 day period to assess strength evolution. Pull-off adhesion tests (illustrated in Fig. 5b) were performed on geopolymer patches according to standard BS EN 1542–1999 to determine the adhesion strength.

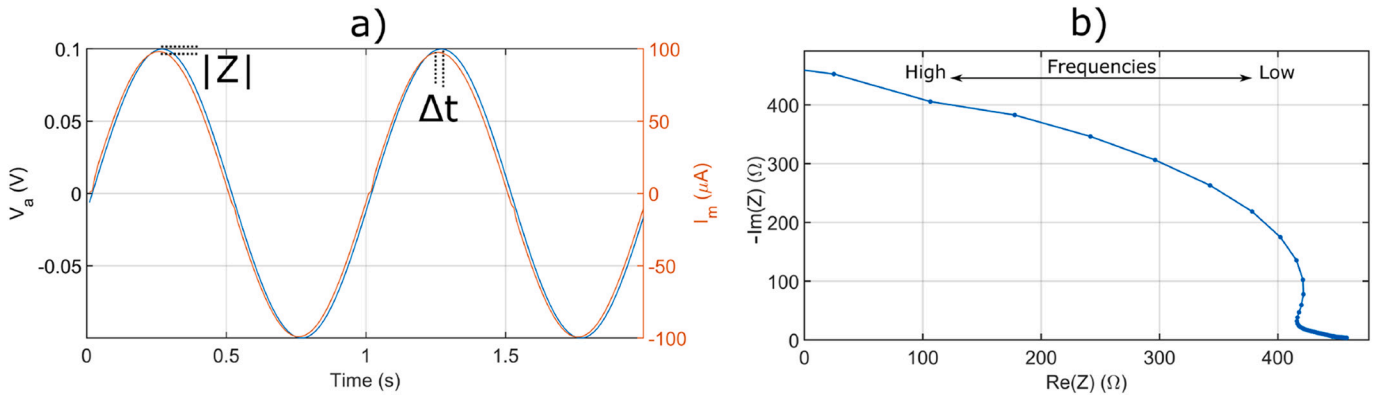

Fig. 3. a) Applied voltage, V_a and measured current, I_m of a geopolymer at 1 Hz applied sinusoid. b) Nyquist plot of a geopolymer patch.

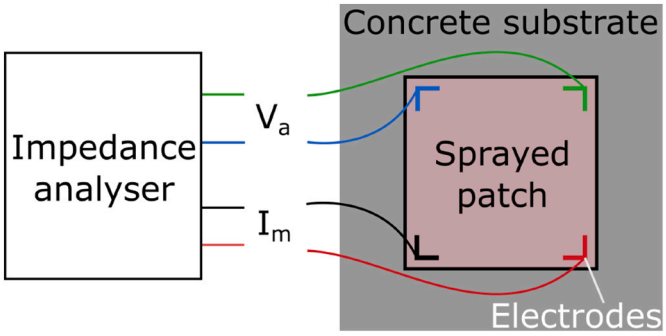

Fig. 4. 4-electrode setup used in this work, with applied voltage V_a and measured current I_m labelled.

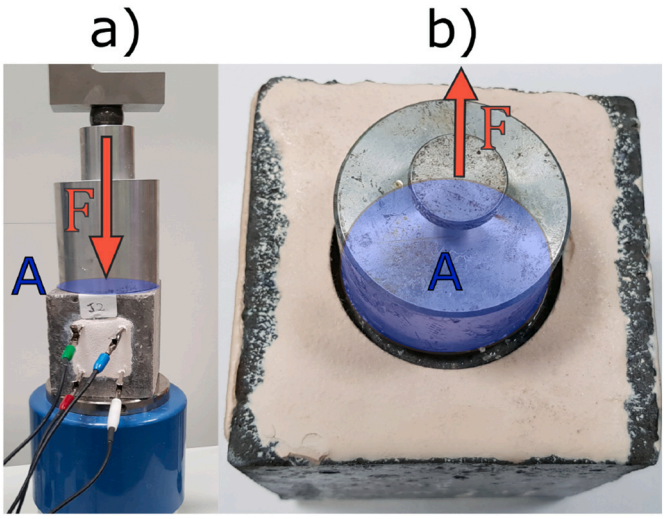

Fig. 5. a) Compression and b) adhesion bond strength experimental set-ups.

3. Results and discussion

3.1. Robotic deposition

Square patches of width, W= 50 mm and thickness H= 2 mm were robotically spray coated onto concrete substrates. An example patch is shown in Fig. 6. Variables of spray coating, listed in Table 3, were optimised for this given patch geometry and the material mix design listed in Section 2.2. Table 3 lists the parameters used in this work and also describes how each variable can affect the robotic spray coating process: it shows, for example, that increased robot head speeds may require increased flow to ensure constant patch thickness. As depicted in Fig. 1b), the spray coating process is made up of fast, sweeping motions and a large number of layers ($L \geq 10$). This approach provides a more thorough coating of the substrate and allows small holes within the concrete surface to be filled with material.

Using the values listed in Table 3, we can achieve reliable spray coating of 50 mm × 50 mm patches within 3 min. The patches in this work were relatively small, simply to stay within the bounds of our experimental rigs. While the thickness of patches was uniform, from Fig. 3 it is clear that patch edges are not precisely deposited. This is due to the random nature of the spraying process. The impact would be less

Fig. 6. Sprayed 50 × 50 mm patch on concrete.

Table 3
Equipment variables that effect patch characteristics.

Variable	Chosen value	Effect on patch
Spray pressure	≈ 0.2 bar	Higher pressure causes "hollow circle" and displaces material, causing uneven patch surfaces
Pump volume flow	0.4 ml/min	High flow rates increase material flow, thus increasing patch thickness
Proximity	1 cm (6 cm for sensor)	Closer proximity can cause "hollow circle", decreases spread of spray
Robot speed & acceleration	1 m/s & 1 m/s^2	Higher speed/acceleration decreases patch thickness
Nozzle diameter	0.5 mm	Larger nozzle increase spread of spray

pronounced for larger patches, required for sensing structures in the field, and could be improved in future work by completely coating faces, or by masking edges.

3.2. Mechanical properties

Cube strength results of the geopolymer mix are shown in Fig. 7 over a 28 day period. This is following a 24 h period at 40 °C to accelerate curing. Day 1 therefore represents the compressive strength subsequent to this curing period. Three samples were tested on each day, with the standard deviation in results represented by the error bars in Fig. 7. After 28 days, this mix reaches a 20 MPa compressive strength. This meets the standard BS EN 1504:1999 for non-structural concrete repairs ($\geq$ 15 MPa). The mechanical strength of the geopolymer material is not the focus of this research. As discussed, in order to obtain sprayability of the material, a low solid/liquid ratio is required. This reduces the compressive strength of the material (due to the excess water in the solution) to lower than conventional metakaolin geopolymers pastes, which can achieve up to 52 MPa [65].

Adhesion bond strength (Fig. 5b) tests were carried out on multiple patches, providing a mean strength of 0.5 MPa $\pm$ 0.1 MPa. This is slightly less than the BS EN 1504–1999 requirements of $\geq$ 0.8 MPa. Reduced adhesion may be the result of the need to pre-wet concrete substrates prior to spraying, to reduce drying shrinkage for our lab scale mix. This reduces penetration of the mix into the concrete. A large scale spray coater capable of spraying mixes containing sand would be able to self-control its shrinkage such that pre-wetting of the concrete is not required. Furthermore, sandblasting of the concrete surface prior to deployment could also improve adhesion.

3.3. Temperature sensing

Fig. 8 shows the fractional shift in impedance response as a function of temperature, with the 95% confidence interval based on 5 samples represented by the shaded region. Here, the baseline impedance, Z_0, is defined as the impedance at 20 °C and an ac current frequency of 500 Hz. A fit using the temperature dependence Eq. (2) was applied. The fit parameters and their standard errors can be found in Table 4. The precision of the temperature measurement is $\delta T = 0.2^{\circ}C$.

As shown, patch impedance response to temperature follows the exponential dependence outlined in Eq. (2), with the largest variance at lower temperatures. As temperature increases, ion migration in the material is accelerated, causing an exponential decrease in impedance [31].

3.4. Strain sensing

The patch-sensor response to applied strain on the concrete cube is shown in Fig. 9. The 95% confidence interval is represented by the shaded region and error bars represent experimental errors. Applied force, F has been converted into an applied strain, ε via:

$$\varepsilon = \frac{F}{EA}, \tag{3}$$

where $E = 20$ GPa is the Young's Modulus of concrete and $A = 0.01$ m^2 is the cross-sectional area of the concrete cube. Strains have been kept low ($< 100\ \mu\varepsilon$) to ensure the concrete remains within its linear elastic region. Increasing this applied strain will cause a non-linear response in both concrete and geopolymer, which makes analysis more difficult. Geopolymers will therefore crack along with the concrete at these higher strains, causing large increases in impedance.

As shown in Fig. 9, the fractional shifts in sensor response are linear under small mechanical loads, with a goodness of fit of $R^2 = 0.9998$. It can be assumed that the applied compressive stress hinders the migration of ions in the material, causing a linear increase in impedance. The fit parameters and their standard errors can be found in Table 4. The strain constant of proportionality is $K_e = 2 \times 10^4$ and this leads to an approximate strain resolution of 1 $\mu\varepsilon$. It is worth noting that the

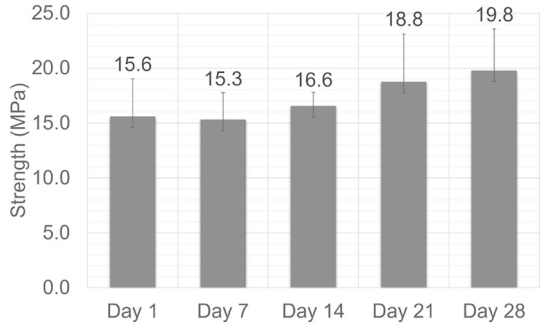

Fig. 7. Compressive strength results for the mix design in this work. Bars show the mean and repeatability of strength results found based on 3 samples at each day.

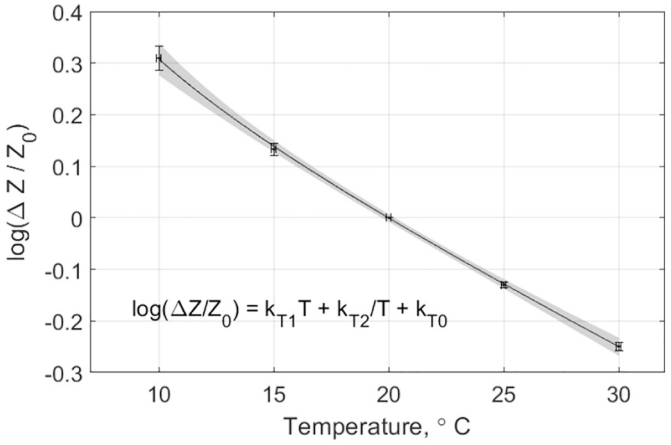

Fig. 8. Sensor response vs temperature, with 95% confidence interval shown as a shaded region based on 5 samples.

Table 4
Characterised temperature and strain sensitivities for use with Eq. (2).

Parameter	Value	Standard error
k_{T1}	−0.023	0.001
k_{T2}	1.8	0.3
k_{T0}	0.35	0.03
k_ε	2×10^4	500

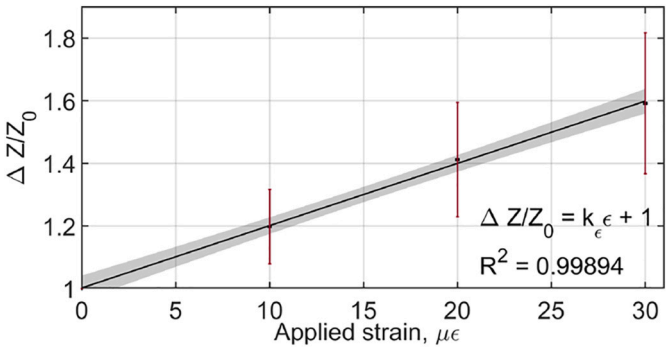

Fig. 9. Sensor response vs applied strain, with 95% confidence interval shown as a shaded region based on the linear fit. Error bars show the standard deviation in sensor response, found over three repeat tests.

precision of the strain measurement will be lower in field conditions, as other measurands affecting the patch (e.g. moisture, chloride etc.) will vary and require measurement to allow for compensation, something which itself bears an error. Compensation for these measurands using a second reference sensor may be required for long-term applications in field conditions. Experimental errors are large. Possible sources of error are: varying sensitivity to force caused by inconsistencies in concrete and geopolymer properties between samples (volume, number of aggregates, density etc.), varying adhesion strengths, and uncompensated fluctuations in humidity during testing. These sources of error will be investigated further in future work.

4. Conclusion

This paper demonstrates, for the first time, the feasibility of robotically spray coating a self-sensing geopolymer material onto concrete substrates. The mechanical properties of the designed mix and its ability to measure both temperature and strain were outlined. Conducting this demonstration at lab scale has imposed challenges: shrinkage of the geopolymer binder had to be controlled without the addition of sand, and the small scale led to imprecision at the edges of the patches. Scaling the process up in future work should allow us to circumvent both of these issues. This work represents our first step in converting the unknown, unchecked human errors and costs associated with sensor/novel material installation into traceable and repeatable robotic errors. We cannot yet guarantee that uncertainties will be reduced using robotics, but we can at least begin to ensure that uncertainties are consistent, traceable and quantified.

Declaration of Competing Interest

The authors declare that they have no known competing financial interests or personal relationships that could have appeared to influence the work reported in this paper.

Acknowledgment

This work was supported in part by the Scottish Funding Council's Oil & Gas Innovation Centre, and the Royal Society (RG160748).

Appendix A. Supplementary data

Supplementary data to this article can be found online at https://doi.org/10.1016/j.autcon.2020.103415.

References

[1] C. Lagat, S. Higgins, C. Otto, Degradation of subsea concrete structures, Online report - last visited 1/9/20 (2019), URL, https://espace.curtin.edu.au/bitstream/handle/20.500.11937/75371/75574.pdf?sequence=2, 2019.
[2] U.S. Department of Transportation, Federal Highway Administration, Status of the nation's Highways, Bridges and Transit: Conditions and Performance, Online Report - Last Visited 1/9/20 (January 2017), URL, https://www.fhwa.dot.gov/policy/2015cpr/, 2015.
[3] S. Ion, Nuclear energy: current situation and prospects to 2020, Philos. Trans. R. Soc. A Math. Phys. Eng. Sci. 365 (1853) (2007) 935–944, https://doi.org/10.1098/rsta.2006.1958.
[4] W. Shanks, C. Dunant, M.P. Drewniok, R. Lupton, A. Serrenho, J.M. Allwood, How much cement can we do without? Lessons from cement material flows in the Uk, Resour. Conserv. Recycl. 141 (2019) 441–454, https://doi.org/10.1016/j.resconrec.2018.11.002. URL. http://www.sciencedirect.com/science/article/pii/S0921344918304191.
[5] National Science and Technology Council, Grand challenges for disaster reduction, Online report - last visited 1/9/20 (June 2005). URL https://www.sdr.gov/grandchallenges.html.
[6] Directorate-General for Mobility and Transport (European Commission), Research theme analysis report: Transport infrastructure, Online report - last visited 1/9/10 (2017), 2017, https://doi.org/10.2832/13882.
[7] T. McDaniels, S. Chang, D. Cole, J. Mikawoz, H. Longstaff, Fostering resilience to extreme events within infrastructure systems: characterizing decision contexts for mitigation and adaptation, Glob. Environ. Chang. 18 (2) (2008) 310–318, https://doi.org/10.1016/j.gloenvcha.2008.03.001. URL. http://www.sciencedirect.com/science/article/pii/S0959378008000174.
[8] A. Durelli, Experimental strain and stress analysis of solid propellant rocket motors, in: A. Eringen, H. Liebowitz, S. Koh, J. Crowley (Eds.), Mechanics and Chemistry of Solid Propellants, Pergamon, 1967, pp. 381–442, https://doi.org/10.1016/B978-1-4831-9837-8.50023-5.
[9] Expedition engineering - Get it right initiative, Research report revision 3, Online report - last visited 1/9/20 (2016), URL, https://getitright.uk.com/reports/research-report, 2016.
[10] Y. Ding, A. Hellmann, L.D. Mello, Factors driving memory fallibility: a conceptual framework for accounting and finance studies, J. Behav. Exp. Financ. 14 (2017) 14–22, https://doi.org/10.1016/j.jbef.2017.03.003. URL.
[11] W. Walker, P. Harremoës, J. Rotmans, J. van der Sluijs, M. van Asselt, P. Janssen, M.K. von Krauss, Defining uncertainty: A conceptual basis for uncertainty management in model-based decision support, Integrated Assess. 4 (1) (2003) 5–17, https://doi.org/10.1076/iaij.4.1.5.16466.
[12] J.H. Porter, P.C. Hanson, C.-C. Lin, Staying afloat in the sensor data deluge, Trends Ecol. Evol. 27 (2) (2012) 121–129, https://doi.org/10.1016/j.tree.2011.11.009. URL. http://www.sciencedirect.com/science/article/pii/S0169534711003326.
[13] F. Moon, Impacts of epistemic (bias) uncertainty on structural identification of constructed (civil) systems, Shock Vibrat. Digest 38 (2006) 399–420, https://doi.org/10.1177/0583102406068068.
[14] L. Biondi, M. Perry, C. Vlachakis, Z. Wu, A. Hamilton, Ambient cured fly ash geopolymer coatings for concrete, Manufact. Process. Syst. (2019), https://doi.org/10.3390/ma12060923.
[15] S. Kramar, A. Šajna, V. Ducman, Assessment of alkali activated mortars based on different precursors with regard to their suitability for concrete repair, Constr. Build. Mater. 124 (2016) 937–944, https://doi.org/10.1016/j.conbuildmat.2016.08.018.
[16] M. Saafi, L. Tang, J. Fung, M. Rahman, F. Sillars, J. Liggat, X. Zhou, Smart Materials and Structures 23, 2014, p. 065006, https://doi.org/10.1088/0964-1726/23/6/065006, 6.
[17] M. Saafi, G. Piukovics, J. Ye, Smart Materials and Structures 25, 2016, p. 105018, https://doi.org/10.1088/0964-1726/25/10/105018, 10.
[18] M. Saafi, A. Gullane, B. Huang, H. Sadeghi, J. Ye, F. Sadeghi, Inherently multifunctional geopolymeric cementitious composite as electrical energy storage and self-sensing structural material, Compos. Struct. 201 (2018) 766–778, https://doi.org/10.1016/j.compstruct.2018.06.101.
[19] M. Perry, M. Saafi, G. Fusiek, P. Niewczas, Hybrid optical-fibre/geopolymer sensors for structural health monitoring of concrete structures, Smart Mater. Struct. (2015), https://doi.org/10.1088/0964-1726/24/4/045011.
[20] A.M. Rashad, Alkali-activated metakaolin: a short guide for civil engineer – an overview, Constr. Build. Mater. 41 (2013) 751–765, https://doi.org/10.1016/j.conbuildmat.2012.12.030.
[21] J.L. Provis, Alkali-activated materials, Cem. Concr. Res. 114 (2018) 40–48, https://doi.org/10.1016/j.cemconres.2017.02.009.
[22] J.L. Provis, S.A. Bernal, Geopolymers and related alkali-activated materials, Ann. Rev. Mater. Res. 44 (1) (2014) 299–327, https://doi.org/10.1146/annurev-matsci-070813-113515.
[23] X.-M. Cui, G.-J. Zheng, Y.-C. Han, F. Su, J. Zhou, A study on electrical conductivity of chemosynthetic al2o3–2sio2 geoplоymer materials, J. Power Sources 184 (2) (2008) 652–656, selected papers from the: INTERNATIONAL BATTERY MATERIALS ASSOCATION 2007 CONFERENCE. In Memoriam of Juergen Besenhard. doi.10.1016/j.jpowsour.2008.03.021.
[24] S. Hanjitsuwan, P. Chindaprasirt, K. Pimraksa, Electrical conductivity and dielectric property of fly ash geopolymer pastes, Int. J. Miner. Metall. Mater. 18 (1) (2011) 94–99, https://doi.org/10.1007/s12613-011-0406-0.
[25] R. Pouhet, M. Cyr, Formulation and performance of flash metakaolin geopolymer concretes, Constr. Build. Mater. 120 (2016) 150–160, https://doi.org/10.1016/j.conbuildmat.2016.05.061. URL.
[26] C. Lamuta, L. Bruno, S. Candamano, L. Pagnotta, Piezoresistive characterization of graphene/metakaolin based geopolymeric mortar composites, MRS Advances 2 (2017) 1–7, https://doi.org/10.1557/adv.2017.595.
[27] P. Rovnaník, I. Kusák, P. Bayer, P. Schmid, L. Fiala, Comparison of electrical and self-sensing properties of Portland cement and alkali-activated slag mortars, Cem. Concr. Res. 118 (2019) 84–91, https://doi.org/10.1016/j.cemconres.2019.02.009.
[28] L. Deng, Y. Ma, J. Hu, S. Yin, X. Ouyang, J. Fu, A. Liu, Z. Zhang, Preparation and piezoresistive properties of carbon fiber-reinforced alkali-activated fly ash/slag mortar, Constr. Build. Mater. 222 (2019) 738–749, https://doi.org/10.1016/j.conbuildmat.2019.06.134.
[29] P. Duxson, J.L. Provis, Designing precursors for geopolymer cements, J. Am. Ceram. Soc. 91 (12) (2008) 3864–3869.
[30] P. Duxson, A. Fernández-Jiménez, J.L. Provis, G.C. Lukey, A. Palomo, J.S.J. van Deventer, Geopolymer technology: the current state of the art, J. Mater. Sci. 42 (9) (2007) 2917–2933.
[31] L. Biondi, M. Perry, J. McAlorum, C. Vlachakis, A. Hamilton, Geopolymer-based moisture sensors for reinforced concrete health monitoring, Sensors Actuators B Chem. 309 (127775) (2020), https://doi.org/10.1016/j.snb.2020.127775.
[32] Y. Wang, Y. Wang, B. Han, B. Wan, G. Cai, Z. Li, Strain monitoring of concrete components using embedded carbon nanofibers/epoxy sensors, Constr. Build. Mater. 186 (2018) 367–378, https://doi.org/10.1016/j.conbuildmat.2018.07.147.
[33] J.H. Shin, H.L. Lee, S.H. Cho, J. Ha, H. Nam, G.S. Cha, Characterization of epoxy resin-based anion-responsive polymers: Applicability to chloride sensing in physiological samples, Anal. Chem. 76 (14) (2004) 4217–4222, https://doi.org/10.1021/ac049973y.

[34] B. Han, L. Zhang, J. Ou, Self-sensing Concrete, in: Smart and Multifunctional Concrete Toward Sustainable Infrastructures, Springer Singapore, Singapore, 2017, pp. 81–116.
[35] L.K. Turner, F.G. Collins, Carbon dioxide equivalent (co2-e) emissions: a comparison between geopolymer and opc cement concrete, Constr. Build. Mater. 43 (2013) 125–130, https://doi.org/10.1016/j.conbuildmat.2013.01.023.
[36] C.L. Page, Corrosion and protection of reinforcing steel in concrete, in: C. Page, M. Page (Eds.), Durability of Concrete and Cement Composites, Woodhead Publishing Series in Civil and Structural Engineering, Woodhead Publishing, 2007, pp. 136–186, https://doi.org/10.1533/9781845693398.136.
[37] S. Falsini, U. Bardi, A. Abou-Hassan, S. Ristori, Sustainable strategies for large-scale nanotechnology manufacturing in the biomedical field, Green Chem. 20 (2018) 3897–3907, https://doi.org/10.1039/C8GC01248B.
[38] B. Panda, S.C. Paul, L.J. Hui, Y.W.D. Tay, M.J. Tan, Additive manufacturing of geopolymer for sustainable built environment, J. Clean. Prod. 167 (2017) 281–288, https://doi.org/10.1016/j.jclepro.2017.08.165.
[39] B. Panda, S.C. Paul, M.J. Tan, Anisotropic mechanical performance of 3d printed fiber reinforced sustainable construction material, Mater. Lett. 209 (2017) 146–149, https://doi.org/10.1016/j.matlet.2017.07.123.
[40] J.H. Lim, B. Panda, Q.-C. Pham, Improving flexural characteristics of 3d printed geopolymer composites with in-process steel cable reinforcement, Constr. Build. Mater. 178 (2018) 32–41, https://doi.org/10.1016/j.conbuildmat.2018.05.010.
[41] G. Ma, Z. Li, L. Wang, G. Bai, Micro-cable reinforced geopolymer composite for extrusion-based 3d printing, Mater. Lett. 235 (2019) 144–147, https://doi.org/10.1016/j.matlet.2018.09.159.
[42] J. Matthews, A. Selvakumar, S. Vaidya, W. Condit, Large-Diameter Sewer Rehabilitation Using a Spray-Applied Fiber-Reinforced Geopolymer Mortar, Practice Periodical on Structural Design and Construction 20 (06 2014), 2014, https://doi.org/10.1061/(ASCE)SC.1943-5576.0000246.
[43] J. Temuujin, A. Minjigmaa, W. Rickard, A. van Riessen, Thermal properties of spray-coated geopolymer-type compositions, J. Thermal Anal. Calorimetr. 107 (1) (2012) 287–292.
[44] J. Temuujin, A. Minjigmaa, W. Rickard, M. Lee, I. Williams, A. van Riessen, Fly ash based geopolymer thin coatings on metal substrates and its thermal evaluation, J. Hazard. Mater. 180 (1) (2010) 748–752, https://doi.org/10.1016/j.jhazmat.2010.04.121.
[45] J. Zhou, G. Ye, K. van Breugel, Cement hydration and microstructure in concrete repairs with cementitious repair materials, Constr. Build. Mater. 112 (2016) 765–772, https://doi.org/10.1016/j.conbuildmat.2016.02.203.
[46] D. Morgan, Compatibility of concrete repair materials and systems, Constr. Build. Mater. 10 (1) (1996) 57–67, https://doi.org/10.1016/0950-0618(95)00060-7.
[47] L. Courard, T. Piotrowski, A. Garbacz, Near-to-surface properties affecting bond strength in concrete repair, Cem. Concr. Compos. 46 (2014) 73–80, https://doi.org/10.1016/j.cemconcomp.2013.11.005.
[48] F. Pacheco-Torgal, J. Castro-Gomes, S. Jalali, Adhesion characterization of tungsten mine waste geopolymeric binder. Influence of opc concrete substrate surface treatment, Constr. Build. Mater. 22 (3) (2008) 154–161, https://doi.org/10.1016/j.conbuildmat.2006.10.005.
[49] C. Zanotti, P.H. Borges, A. Bhutta, N. Banthia, Bond strength between concrete substrate and metakaolin geopolymer repair mortar: effect of curing regime and pva fiber reinforcement, Cem. Concr. Compos. 80 (C) (2017) 307–316, https://doi.org/10.1016/j.cemconcomp.2016.12.014.
[50] R. Pouhet, M. Cyr, R. Bucher, Influence of the initial water content in flash calcined metakaolin-based geopolymer, Constr. Build. Mater. 201 (2019) 421–429, https://doi.org/10.1016/j.conbuildmat.2018.12.201.
[51] Changzhou Tian Yi Engineering Fiber Co, Pva fibre datasheet, Online report - last visited 1/9/20, URL, https://tianyifiber.en.made-in-china.com/product/kvBQXnDcfSWM/China-High-Quality-Faint-Yellow-PVA-Cutting-Fiber-3mm-19mm.html.
[52] Nycon, Pva fibre datasheet, Online report - last visited 1/9/20, URL, https://nycon.com/collections/pva-fibers.
[53] A.M. Rashad, Metakaolin as cementitious material: history, scours, production and composition – a comprehensive overview, Constr. Build. Mater. 41 (2013) 303–318, https://doi.org/10.1016/j.conbuildmat.2012.12.001.
[54] C. Vlachakis, M. Perry, L. Biondi, J. McAlorum, 3d printed temperature-sensing repairs for concrete structures, Additive Manufacturing 34 (101238) (2020), https://doi.org/10.1016/j.addma.2020.101238.
[55] C. Kuenzel, L.J. Vandeperre, S. Donatello, A.R. Boccaccini, C. Cheeseman, Ambient temperature drying shrinkage and cracking in metakaolin-based geopolymers, J. Am. Ceram. Soc. 95 (10) (2012) 3270–3277.
[56] Z. Zhang, X. Yao, H. Wang, Potential application of geopolymers as protection coatings for marine concrete iii. field experiment, Appl. Clay Sci. 67–68 (2012) 57–60.
[57] J.J. Ekaputri, S. Junaedi, Wijaya, Effect of curing temperature and fiber on metakaolin-based geopolymer, Proc. Eng. 171 (2017) 572–583, the 3rd International Conference on Sustainable Civil Engineering Structures and Construction Materials - Sustainable Structures for Future Generations.
[58] M. Manfaluthy, J. Ekaputri, The application of pva fiber to improve the mechanical properties of geopolymer concrete, in: MATEC Web of Conferences, January 2017, p. 138, https://doi.org/10.1051/matecconf/201713801020.
[59] E. Vasconcelos, S. Fernandes, J.B. de Aguiar, F. Pacheco-Torgal, Concrete retrofitting using metakaolin geopolymer mortars and cfrp, Constr. Build. Mater. 25 (8) (2011) 3213–3221, https://doi.org/10.1016/j.conbuildmat.2011.03.006.
[60] A.M. Aguirre-Guerrero, R.A. Robayo-Salazar, R. M. de GutiÃ©rrez, A novel geopolymer application: Coatings to protect reinforced concrete against corrosion, Appl. Clay Sci. 135 (2017) 437–446, https://doi.org/10.1016/j.clay.2016.10.029.
[61] A.M. Rashad, Effect of quartz-powder on the properties of conventional cementitious materials and geopolymers, Mater. Sci. Technol. 34 (17) (2018) 2043–2056.
[62] P. Duan, C. Yan, W. Luo, W. Zhou, Effects of adding nano-tio2 on compressive strength, drying shrinkage, carbonation and microstructure of fluidized bed fly ash based geopolymer paste, Constr. Build. Mater. 106 (2016) 115–125, https://doi.org/10.1016/j.conbuildmat.2015.12.095.
[63] M. Perry, M. Saafi, G. Fusiek, P. Niewczas, Geopolymeric thermal conductivity sensors for surface-mounting onto concrete structures, in: 9th International Concrete Conference 2016: Environment, Efficiency and Economic Challenges for Concrete, 2016. URL, https://strathprints.strath.ac.uk/id/eprint/60745.
[64] L.J. van der Pauw, A method of measuring specific resistivity and hall effect of discs of arbitrary shape, Philips Res. Rep. 13 (1958), https://doi.org/10.1142/9789814503464_0017.
[65] Z. W. Y. F. J. Chen, L. Wang, Preparation and properties of alkali activated metakaolin-based geopolymer, Materials (2016), https://doi.org/10.3390/ma9090767.